Journal of Membrane Science 520 (2016) 281–293

Contents lists available at ScienceDirect

Journal of Membrane Science

journal homepage: www.elsevier.com/locate/memsci

Photocatalytic antifouling PVDF ultrafiltration membranes based on synergy of graphene oxide and TiO_2 for water treatment

Zhiwei Xu [a,*], Tengfei Wu [a], Jie Shi [b], Kunyue Teng [b], Wei Wang [b], Meijun Ma [b], Jing Li [b], Xiaoming Qian [b,*], Cuiyu Li [b], Jintu Fan [b]

[a] State Key Laboratory of Separation Membranes and Membrane Processes, School of Textiles, Tianjin Polytechnic University, Tianjin 300387, China
[b] School of Textiles, Tianjin Polytechnic University, Tianjin 300387, China

ARTICLE INFO

Article history:
Received 10 May 2015
Received in revised form
28 July 2016
Accepted 28 July 2016

Keywords:
Graphene oxide
TiO_2
Hybrid membrane
Photodegradation
Self-cleaning

ABSTRACT

A novel graphene oxide/TiO_2-polyvinylidene fluoride (GO/TiO_2-PVDF) hybrid ultrafiltration membrane has been successfully developed via the phase inversion technique by supplementing with GO/TiO_2 nanocomposites, in which the synergistic coupling of GO and TiO_2 could result in improved photocatalytic activity and endow hybrid membranes with photocatalytic antifouling function. Compared with PVDF membranes supplemented with TiO_2 and GO, respectively, the GO/TiO_2-PVDF membrane displayed significantly improved photodegradation efficiency (improved about 50–70%) and superior photodegradation kinetics (1.0–1.5 times faster) toward bovine serum albumin (BSA). Moreover, flux performance and flux recovery ratio of membranes revealed that the GO/TiO_2-PVDF membrane could recover high flux after fouling, which thus presented self-cleaning property under UV static irradiation. Besides, the GO/TiO_2-PVDF membrane showed a water flux up to 487.8 L m^{-2} h^{-1}, more than 2 times that of the pristine PVDF membrane, while keeping high BSA rejection (92.5%). Therefore, the GO/TiO_2-PVDF membrane would have good potential in water treatment due to its high-performance multifunctional characters, *i.e.* separation, photocatalytic oxidation and self-cleaning, etc.

1. Introduction

Ultrafiltration technology has emerged as an effective approach for applications in water and wastewater treatment fields in view of its outstanding performance in the removal of various water contaminants [1,2]. Despite these advances, membrane fouling, which can cause reduction in separation performance and shorten membrane life, remains a major obstacle in broadening its applications from an economic or technical point of view [3,4]. Polymeric membranes are the key component for ultrafiltration membranes with regard to their low-cost, high efficiency and high flexibility but their hydrophobic nature is prone to membrane fouling [5–7]. Therefore, various strategies have been performed to control/minimize membrane fouling including blending modification and surface modification [8–11].

Recent advances in polymer-blended modifications have been directed toward the incorporation of inorganic nanomaterials with casting solution to fabricate organic–inorganic hybrid membranes due to their facile processability and stable performance [12]. Nanoparticles such as ZnO [13], SiO_2 [14], Al_2O_3 [15,16], ZrO_2 [17,18], TiO_2 [19–21], $TiSiO_4$ [22], Fe_3O_4 [23], Ag [24], zeolite [25], attapulgite [26] and carbon nanotubes [61–63] are preferred to modify polymeric membranes. Among them, TiO_2 holds great potential due to its innocuity, low-cost, photocatalytic and superhydrophilicity effects [27]. The role of TiO_2 is to tailor the permeability, improve surface hydrophilicity, enhance contaminant removal under ultraviolet (UV) light, and accentuate self-cleaning/antifouling property of membranes [28–30]. However, the strong aggregation tendency of TiO_2 in polymer matrix due to the high surface energy [31] and the low photocatalytic efficiency due to the rapid charge recombination rate within TiO_2 particles [32] are main concerns that impede its feasible application in the ultrafiltration technology. Hence, some approaches have been devoted to address such problems, including metal or nonmetal doping [33,34], coupling with other semiconductors [35], and combining with carbon materials [36–40]. In particular, the combination of TiO_2 with graphene oxide (GO) or reduced graphene oxide (rGO) is considered as a practical way to conquer the above-mentioned problems due to their unique properties [41,42].

The emerging GO is another potential candidate for modification of polymeric membranes [43,44]. Besides, with its large surface area and high charge carrier mobility [45,46], GO is also an ideal nanomaterial for attaching TiO_2 and enhancing the

* Corresponding authors.
E-mail addresses: xuzhiwei@tjpu.edu.cn (Z. Xu), qianxiaoming@tjpu.edu.cn (X. Qian).

http://dx.doi.org/10.1016/j.memsci.2016.07.060
0376-7388/

photocatalytic efficiency of TiO_2. The coupling of GO and TiO_2 in the synthesis of GO/TiO_2 nanocomposites has been well-documented in literature reports [47,48] and the GO/TiO_2 nanocomposites presents thus practical advantages: (i) The large surface area and the abundant oxygen-containing functional groups in GO make them as an extraordinary platform for anchoring TiO_2 and establishing a longer, closer contact between TiO_2 and the contaminant, which may decrease the aggregation [49] and enhance the photocatalytic efficiency of GO/TiO_2 nanocomposites [50]; (ii) The electronic properties of GO can facilitate electron transfer and reduce carrier recombination, eventually achieving an improved photocatalytic efficiency of GO/TiO_2 nanocomposites [51].

To date, there have been a number of efforts toward the introduction of GO/TiO_2 nanocomposites on the surface of membranes to endow membranes with desired characters [52–55]. However, due to the inherent limitations of membrane surface modification, the release of particles from the membrane may still raise problems during long filtration period [19]. Alternatively, blending modification is an intriguing approach with an advantage of easy preparation and effective anchoring of the particles on the polymer matrixes. So far, the integration of GO/TiO_2 nanocomposites in the matrix to fabricate mixed matrix membranes is still in its infancy. Vatanpour and his group focused on this topic and the effects of rGO/TiO_2 nanocomposites with different molar ratios on the performance of polymer-based ultrafiltration/nanofiltration membranes were investigated [49,56,57]. Kumar et al. used the synthesized GO-TiO_2 nanocomposites as a filler to fabricate novel hybrid ultrafiltration membranes for humic acid removal [58]. However, no prior work regarding the photocatalytic property of GO/TiO_2–based membranes has been reported. Hence, regarding the advantages of GO/TiO_2 nanocomposites, by introducing GO/TiO_2 nanocomposites into membrane matrix to form hybrid membranes, it is expected that the synergetic effects of GO and TiO_2 on photocatalytic efficiency can lead to a high-performance photocatalytic antifouling membrane.

To this end, GO/TiO_2 nanocomposites were firstly synthesized by a facile hydrothermal method. Then GO/TiO_2–polyvinylidene fluoride (GO/TiO_2-PVDF) hybrid ultrafiltration membranes were developed from the blending solutions of PVDF and GO/TiO_2 nanocomposites via solution casting and phase inversion method. We have investigated not only the effect of GO/TiO_2 nanocomposites on membrane performance, morphology, and antifouling properties but also the behavior of photocatalytic property based on the photodegradation of bovine serum albumin and fouling mitigation capacity under UV light irradiation, for the first time of hybrid membranes to our knowledge. Membrane characterizations were confirmed in terms of field emission scanning electron microscopy, X-ray photoelectron spectroscopy, atomic force microscopy, water contact angle measurement, pure water flux, rejection and others.

2. Experimental

2.1. Materials

Graphite powder was purchased from Qingdao Ruisheng Graphite Co., Ltd. Nano-sized TiO_2 (P25, 50 nm) was purchased from Aladdin Industrial Corporation. PVDF (FR-904) was purchased from Shanghai 3F New Materials Co., Ltd and was dried at 80 °C for 12 h prior to use. Polyvinyl pyrrolidone (PVP) and N,N-dimethylacetamide (DMAc) were the products of Tianjin Kermel Chemical Co., Ltd. Bovine serum albumin (BSA, M_W=68,000) was obtained from Beijing Biohao Biotechnology Co., Ltd. All other analytical grade reagents, such as H_2SO_4, $KMnO_4$, H_2O_2 and ethanol, were supplied by Tianjin No. 3 Chemical Plant and used without further purification.

2.2. Preparation of GO/TiO_2 nanocomposites

Graphite oxide was synthesized via a modified Hummers' method [59]. After the exfoliation by ultrasonicating 1.0 g L^{-1} of graphite oxide aqueous dispersion for 2.5 h (100 W, 25 kHz), water-soluble and individual GO was recovered by lyophilization. More information on the details of GO synthesis can be found in our previous works [60,61].

The GO/TiO_2 nanocomposites were synthesized according to a facile one-step hydrothermal method [62] with a slight modification. In brief, GO (1.5 mg) was dissolved in a mixed solution containing 20 mL ethanol and 10 mL deionized water by ultrasonication for 1 h, and TiO_2 (13.5 mg) was added to the above mixture and stirred constantly for another 2 h to form homogeneous suspension. Next, the suspension was transferred into an 80 mL Teflon-lined stainless steel autoclave and reacted at 120 °C for 3 h to deposit TiO_2 on the carbon substrate. Afterwards, the resultant product was recovered by centrifugation, rinsed with deionized water and vacuum-dried at 60 °C for 24 h.

2.3. Preparation of GO/TiO_2-PVDF hybrid ultrafiltration membranes

The preparation of PVDF hybrid ultrafiltration membranes via solution casting and phase inversion method is based on previous published papers [63–65] with some modification. Typically, a predesigned recipe of GO/TiO_2 nanocomposites, PVDF and PVP (used as the porogen) was dissolved in DMAc under ultrasonication and agitation to form a homogeneous casting solution and the mixture was further continuously stirred at 50 °C for 24 h. After bubble removal, the solution was spread onto a glass plate and horizontally transferred to a water coagulation bath at 30 °C for 48 h to remove the residual solvent. Upon complete coagulation, the resultant membranes were soaked in deionized water prior to further utilization. For comparison, GO-PVDF membranes, TiO_2-PVDF membranes and pristine PVDF membranes were prepared with the same method as mentioned above following the recipes in Table 1.

2.4. Characterization of GO/TiO_2 nanocomposites

The morphology and microstructure of nanocomposites were characterized by field emission scanning electron microscopy (SEM, Hitachi S-4800), transmission electron microscopy (TEM, TecnaiG2F20) and high-resolution TEM (HRTEM, TecnaiG2F20). The crystal phase was determined by X-ray Diffraction (XRD, Bruker D8 Discover) with Cu Kα radiation (1.54059 Å). The chemical composition was analyzed by X-ray photoelectron spectroscopy (XPS, PHI 5700) with Al Kα excitation radiation (1486.6 eV).

2.5. Characterization of GO/TiO_2-PVDF hybrid ultrafiltration

Table 1
Compositions of casting solution.

Membrane	PVDF (wt%)	PVP (wt%)	Additives		DMAc (wt%)
			Nanomaterials	Amounts (wt%)	
PVDF	15	1	–	–	84
GO-PVDF	15	1	GO	1	83
TiO_2-PVDF	15	1	TiO_2	1	83
GO/TiO_2-PVDF	15	1	GO/TiO_2	1	83

membranes

2.5.1. Characterization of membranes

The top surface and cross-section morphologies of membranes were characterized by SEM after the samples were fractured in liquid nitrogen and gold-sputtered. Energy dispersive X-ray (EDX) spectroscopy being attached to SEM was performed to analyze the element composition. The surface roughness of membranes was investigated by atomic force microscope (AFM, CSPM5500) with a non-contact mode. Roughness parameters such as root-mean-square roughness (*Rq*), mean roughness (*Ra*) and maximum roughness difference (*Rz*) were quantified from the topography images of 10 μm × 10 μm area. The surface hydrophilicity of membranes was conducted by a contact angle goniometer (JC2000D1, China). The membrane porosity ε (%) was calculated by gravimetric method [56] and mean pore size r_m (nm) was determined using Guerout–Elford–Ferry equation [49,56] based on the data of porosity and pure water flux. To minimize the experimental error, all the reported values were based on at least five repeats.

2.5.2. Permeation and separation of membranes

Pure water flux of membranes with an effective area of 19.3 cm^2 was conducted on a dead-end membrane system. Both the pure water flux and rejection tests were directed at 25 °C with a feed pressure of 0.1 MPa and all the reported values were based on at least five repeats. Prior to water flux testing, the membranes were compacted at 0.15 MPa for 1 h. Then the water flux, J (L m^{-2} h^{-1}), was measured at 0.1 MPa and calculated by Eq. (1).

$$J = \frac{Q}{A \times T} \tag{1}$$

where Q (L) is the total volume penetrating through the membrane during the operation time T (h) with an effective filtration area of A (m^2).

The rejection was investigated with 1.0 g L^{-1} BSA solution using 0.1 M phosphate buffered at pH 7.4. To minimize concentration polarization, we settled the stirring rate of BSA solution at 400 rpm, under which stirring speed the effect of concentration polarization can be restricted effectively [63,66]. By monitoring the concentrations of BSA in permeation and feed solutions using a UV spectrophotometer at 280 nm, the BSA rejection, R (%), was estimated by Eq. (2).

$$R(\%) = \left(1 - \frac{C_P}{C_F}\right) \times 100 \tag{2}$$

where C_P and C_F represent the concentrations of BSA in permeation and feed solution, respectively.

2.5.3. Photocatalytic property of membranes

The photocatalytic performance of GO/TiO_2-PVDF membranes and the three control membranes were assessed by monitoring the decrease in concentration of BSA at regular intervals using a UV spectrophotometer (UV-1800, Mapada) during exposure to UV light irradiation (365 nm, 11 W, and the light intensity of 605 μW cm^{-2}). First, the membrane was mounted onto glass slides using double-sided tape to ensure a flat membrane surface. Then the glass slides were immersed in a petri dish which was filled with 50 mL of BSA solution (1.0 g L^{-1}). Before commencing the UV lamp, the solution was in darkness for 60 min to establish adsorption equilibrium.

2.5.4. Fouling analysis and self-cleaning evaluation of membranes

For the fouling resistance analysis, the experiments included three filtration steps were conducted following the procedure according to our previous reports [66]. Briefly, in the first step, the pure water permeability (Jw_1) was measured until the flux remained stable. Then, 1.0 g L^{-1} BSA solution was fed into the filtration system and the flux (Jp) was measured for 1 h. In the final step, following BSA filtration, the fouled membranes were rinsed by deionized water to remove loose bound protein and the water flux (Jrw) of fouled membranes measured after removing loose bound protein was measured. Then the membranes were irradiated for 30 min under the UV lamp to remove pollutant on membrane pore wall or surface before measuring the water flux of the cleaned membranes (Jw_2). Control experiments were also carried out without UV under identical conditions. Filtration resistance-in-series model was given below [13,29]:

$$R_{tot} = \frac{TMP}{\mu J_p} = R_m + R_c + R_f + R_b \tag{3}$$

where TMP is the trans membrane pressure (0.1 MPa) , μ is the viscosity of water at room temperature (1.005×10^{-3} Pa s), and R_{tot} is the total filtration resistance (m^{-1}).

It is also postulated that total filtration resistance is the sum of intrinsic membrane resistance (R_m), cake resistance (R_c) (due to loosely bound protein layer formed on membrane surface), fouling resistance (R_f) (due to strong adsorption of protein on membrane pore wall or surface) and block resistance (R_b) (due to inner pore plugging and irreversible adsorption of protein). The fouling resistance R_f was evaluated by exposing the fouled membrane (after removing the loose protein cake layer) under the UV lamp irradiation for 30 min. These resistances can be calculated using the following Eqs. (4)– (7).

$$R_m = \frac{TMP}{\mu J_{w_1}} \tag{4}$$

$$R_c = R_{tot} - \frac{TMP}{\mu J_{rw}} \tag{5}$$

$$R_f = R_{tot} - R_c - \frac{TMP}{\mu J_{w_2}} \tag{6}$$

$$R_b = R_{tot} - R_m - R_c - R_f \tag{7}$$

To further analyze the fouling process, several equations were introduced to describe the fouling resistance of membranes. The flux recovery ratio (FRR), the total fouling ratio (Rt), reversible fouling ratio (Rr) and irreversible fouling ratio (Rir) were determined as follows [67,68]:

$$FRR(\%) = \frac{Jw_2}{Jw_1} \times 100 \tag{8}$$

$$Rt(\%) = (1 - \frac{Jp}{Jw_1}) \times 100 \tag{9}$$

$$Rr(\%) = (\frac{Jw_2 - Jp}{Jw_1}) \times 100 \tag{10}$$

$$Rir(\%) = (\frac{Jw_1 - Jw_2}{Jw_1}) \times 100 = Rt - Rr \tag{11}$$

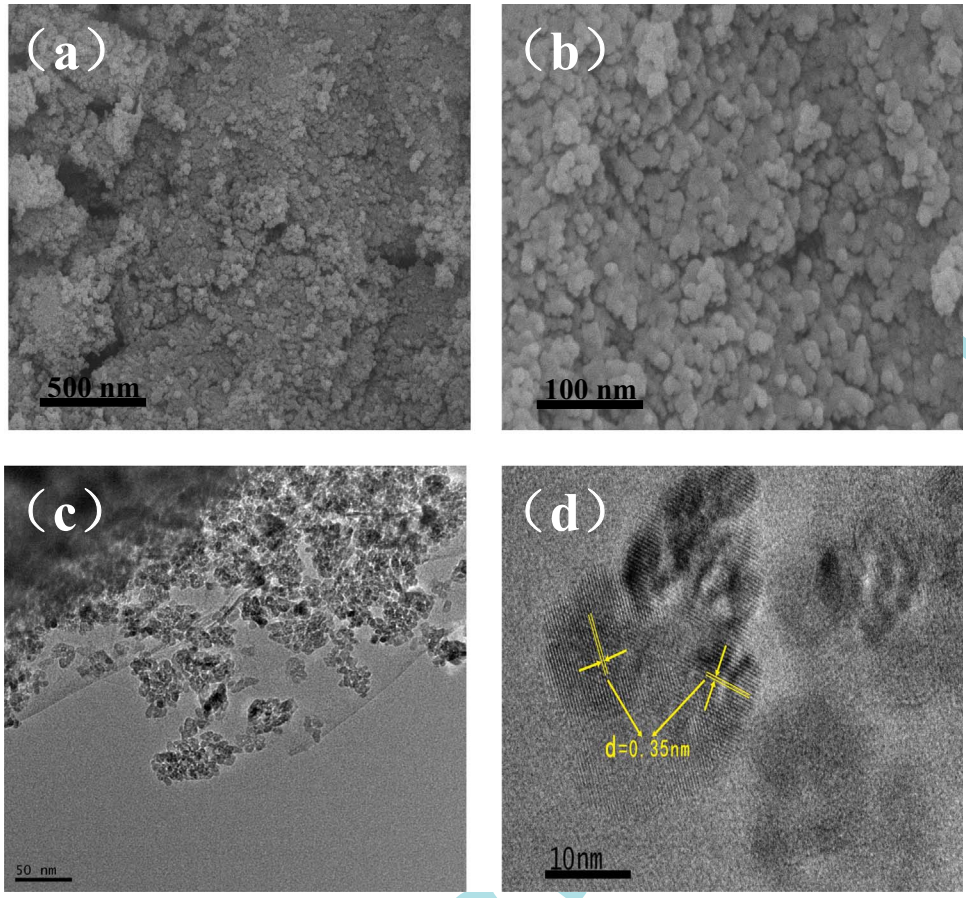

Fig. 1. SEM (a) and (b), TEM (c) and HRTEM (d) images of GO/TiO_2 nanocomposites.

3. Results and discussion

3.1. Characterization of GO/TiO_2 nanocomposites

The microstructures of GO/TiO_2 nanocomposites were well illustrated by SEM and TEM. The morphological SEM images of GO/TiO_2 nanocomposites displayed that TiO_2 and GO were uniformly recombined in nanoscale dimension throughout the morphology, as seen in Fig. 1a and b. The TiO_2 nanoparticles which were attached onto the surface of GO sheets may hinder the restacking of GO sheets, whilst the wimple structure of GO sheets may decrease the aggregation of TiO_2 nanoparticles [56]. As TEM images depicted in Fig. 1c, the nanosized TiO_2 was distributed on the surface of GO sheets, forming relatively uniform GO/TiO_2 composite sheets. The corresponding HRTEM image (Fig. 1d) revealed that the (101) crystal lattice spacing of TiO_2 was measured to be around 0.35 nm, which suggested that the TiO_2 nanoparticles on GO sheets were of good crystallinity. Hence, based on the results of SEM and TEM analyses, TiO_2 nanoparticles were tightly anchored onto the GO sheets, which will be beneficial for photodegradation activity of GO/TiO_2 nanocomposites.

The XRD patterns of GO, TiO_2 and GO/TiO_2 were shown in Fig. 2a. A sharp peak around 10° in the XRD pattern of GO was associated with the (001) inter-layer structure of GO sheets. For TiO_2, the diffraction peaks at 25.3, 37.8, 47.9, 53.8, 55.0, 62.9, 68.7, 70.3 and 75.2° can be indexed to the anatase phase [52], consistent with the HRTEM result (Fig. 1d). The XRD pattern of GO/TiO_2 nanocomposites showed no obvious differences with that of TiO_2, whilst no (001) diffraction of GO was observed, thus implying that the regular stack of GO may be destroyed by intercalation of TiO_2 nanoparticles [50]. Furthermore, the wide-survey and C1s and Ti2p XPS spectra of GO/TiO_2 nanocomposites also confirmed the existence of Ti elements and GO in the as-synthesized samples [69], as depicted in Fig. 2b–d. All the characterization results illustrated the successful synthesis of GO/TiO_2 nanocomposites.

3.2. Morphology and structure of membranes

The top, bottom and cross section views of membranes were compared in Fig. 3, as observed by SEM. All the membranes presented a typical asymmetric microstructure including a dense skin layer supported by numerous macrovoids (sub layer). No distinct variations in the top surface of membranes were observed and all the top surfaces seemed to be flat and smooth, indicating that the structures of top surface were not altered by the addition of inorganic nanomaterials. However, with the supplementation of GO, TiO_2 and GO/TiO_2 into the polymer matrix, the cross section of various membranes formed wider pore channels, whereas the bottom surfaces appeared enlarged pores, compared with pristine PVDF membranes. Instantaneous liquid-liquid phase demixing is responsible for the amelioration of macrovoid formation [13]. Since the hydrophilic nature of GO, TiO_2 and GO/TiO_2 accelerated the exchange of solvent and non-solvent, a large porous structure formed for the hybrid membranes. Compared with pristine PVDF membranes, the similar amelioration in surface porosity and cross-sectional structure could be noted for GO-PVDF and TiO_2-PVDF membranes, but not as palpable as for GO/TiO_2-PVDF membranes. For GO/TiO_2-PVDF membranes, the macroporous substructures and enlarged surface macrovoids compared with the other membranes could be viewed visually from the SEM pictures. This phenomenon could be interpreted as the improved demixing process due to the stronger hydrophilic characteristic of GO/TiO_2

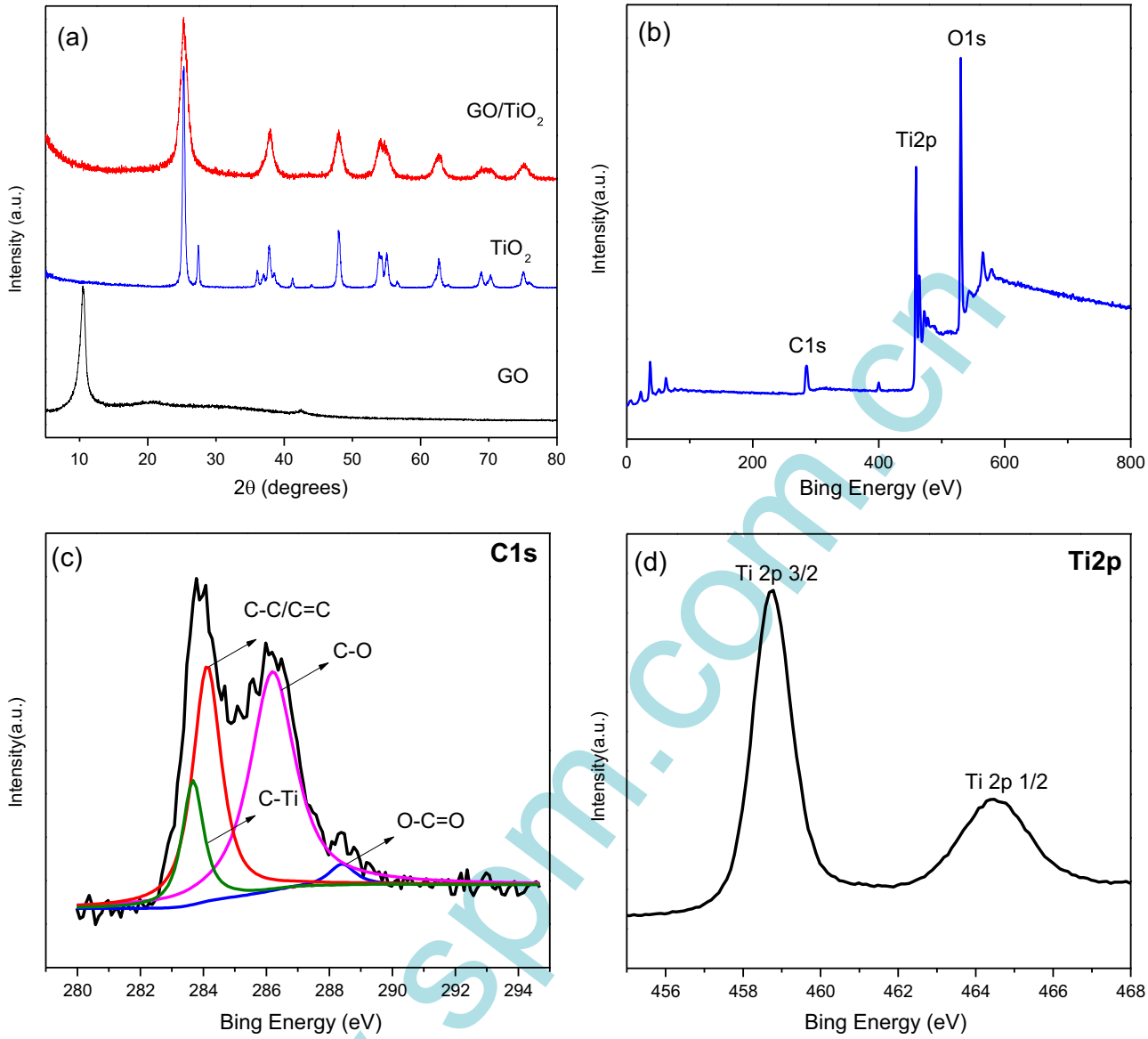

Fig. 2. (a) XRD patterns of GO, TiO_2 and GO/TiO_2 nanocomposites; XPS spectra of GO/TiO_2 nanocomposites: (b) full survey, (c) C1s spectrum and (d) Ti2p spectrum.

compared with inorganic GO and TiO_2. These results were also in accordance with the porosity and pore size data listed in Table 2. It was observed that the GO/TiO_2-PVDF membrane represented the bigger pore and higher porosity than the other three control membranes, which was consistent with the analysis of membrane morphology.

Furthermore, SEM–EDX mapping scanning spectra for membrane surface of carbon (C), fluorine (F), oxygen (O) and titanium (Ti) elements were carried out to explore the presence and distribution of GO/TiO_2 nanocomposites in the GO/TiO_2-PVDF membrane matrix, as observed in Fig. 4. It is noted that the Ti element uniformly distributed in the GO/TiO_2-PVDF membrane, indicating the homogeneous dispersion of GO/TiO_2 nanocomposites within the GO/TiO_2-PVDF membrane matrix.

AFM was used to probe the surface characteristic of membranes, as demonstrated in Fig. 5. According to the AFM images and the corresponding roughness parameters presented in Table 2, the surface roughness of the hybrid membranes, employing *Ra*, *Rq* and *Rz*, displayed an apparent decrease trend compared with that of pristine PVDF membranes. The *Ra* value decreased from 42.7 nm (PVDF) to 15.4 nm (GO-PVDF), 12.3 nm (TiO_2-PVDF) and 10.4 nm (GO/TiO_2-PVDF), which was possibly due to the presence of inorganic nanomaterials within the concavities of the hybrid membrane surface. Vatanpour et al. [49,56] also reported the similar behavior for rGO/TiO_2-PVDF hybrid membranes. It is generally deemed that a membrane with smoother surface possesses greater antifouling capability [11,70]. Therefore, the PVDF hybrid membranes turned out the potential antifouling tendency, which was consistent with the flux recovery results of the membranes depicted in the later part.

3.3. Hydrophilicity of membranes

Surface hydrophilicity is a significant factor in determining the flux and antifouling performance of membranes. The hydrophilicity of membrane surface was understood based on water contact angle measurement by the sessile drop technique. In general, smaller water contact angle refers to higher hydrophilicity. Compared in Fig. 6 were the contact angle results of various membranes. Supplementation of the membrane with GO, TiO_2 and GO/TiO_2 tended to considerably decrease the water contact angle. Pristine PVDF membranes possessed highest water

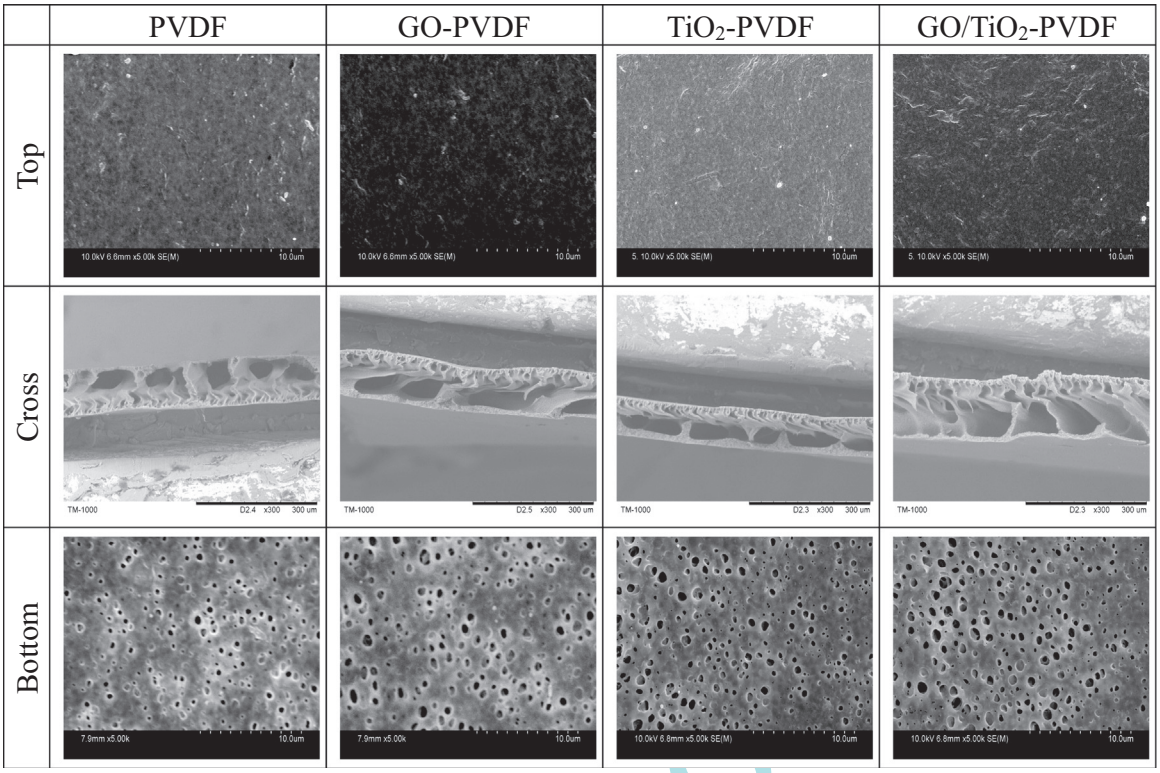

Fig. 3. SEM images top surface,cross section and bottom surface morphology: PVDF, GO-PVDF, TiO_2-PVDF and GO/TiO_2-PVDF membranes.

Table 2
Porosity, surface mean pore size and roughness parameters of membranes.

Membrane	Porosity (%)	Mean pore size (nm)	Roughness		
			Ra (nm)	*Rq* (nm)	*Rz* (nm)
PVDF	69.6	48.1	42.7	55.2	416
GO-PVDF	78.3	55.7	15.4	20.3	184
TiO_2-PVDF	75.1	52.6	12.3	15.6	143
GO/TiO_2-PVDF	83.1	65.2	10.4	12.7	108

contact angle of $79 \pm 1.3°$, whereas GO-PVDF, TiO_2-PVDF and GO/TiO_2-PVDF hybrid membranes achieved water contact angles of $68 \pm 1.5°$, $65 \pm 1.0°$ and $61 \pm 0.8°$, respectively. The amelioration of hybrid membrane hydrophilicity may be ascribed to the spontaneous migration of hydrophilic nanomaterials moving towards the membrane/water interface to decrease the interface energy during the phase inversion process [71–73]. Note that the contact angle of TiO_2-PVDF membranes was slightly smaller than that of GO-PVDF membranes. The high affinity of TiO_2 to water and hydrolysis with hydroxyl groups owing to the presence of TiO_2 nanoparticles is responsible for this behavior [74]. Same tendency was also observed by Vatanpour for TiO_2-PVDF membranes and GO-PVDF membranes [49,56]. In contrast with the other membranes, GO/TiO_2-PVDF membranes achieved the lowest contact angle, which was mainly attributed to the hydrophilic properties of the GO/TiO_2 nanocomposites. Besides, since the water contact angle was measured by the sessile drop technique under sunlight for a few tens of seconds, the sunlight irradiation could further reduce the water contact angles of GO/TiO_2-PVDF hybrid membranes due to the photo-induced hydrophilicity of TiO_2, which also contributed to the lowest contact angle, albeit to a small extent [55]. This may act favorably in promoting water permeability and antifouling properties (discussed later).

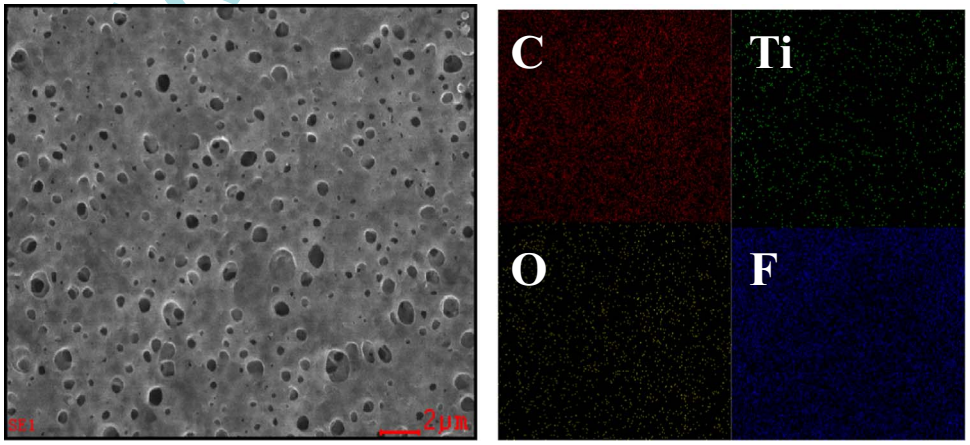

Fig. 4. SEM images of GO/TiO_2-PVDF membranes and corresponding EDX mapping scanning spectra of C, Ti, O and F.

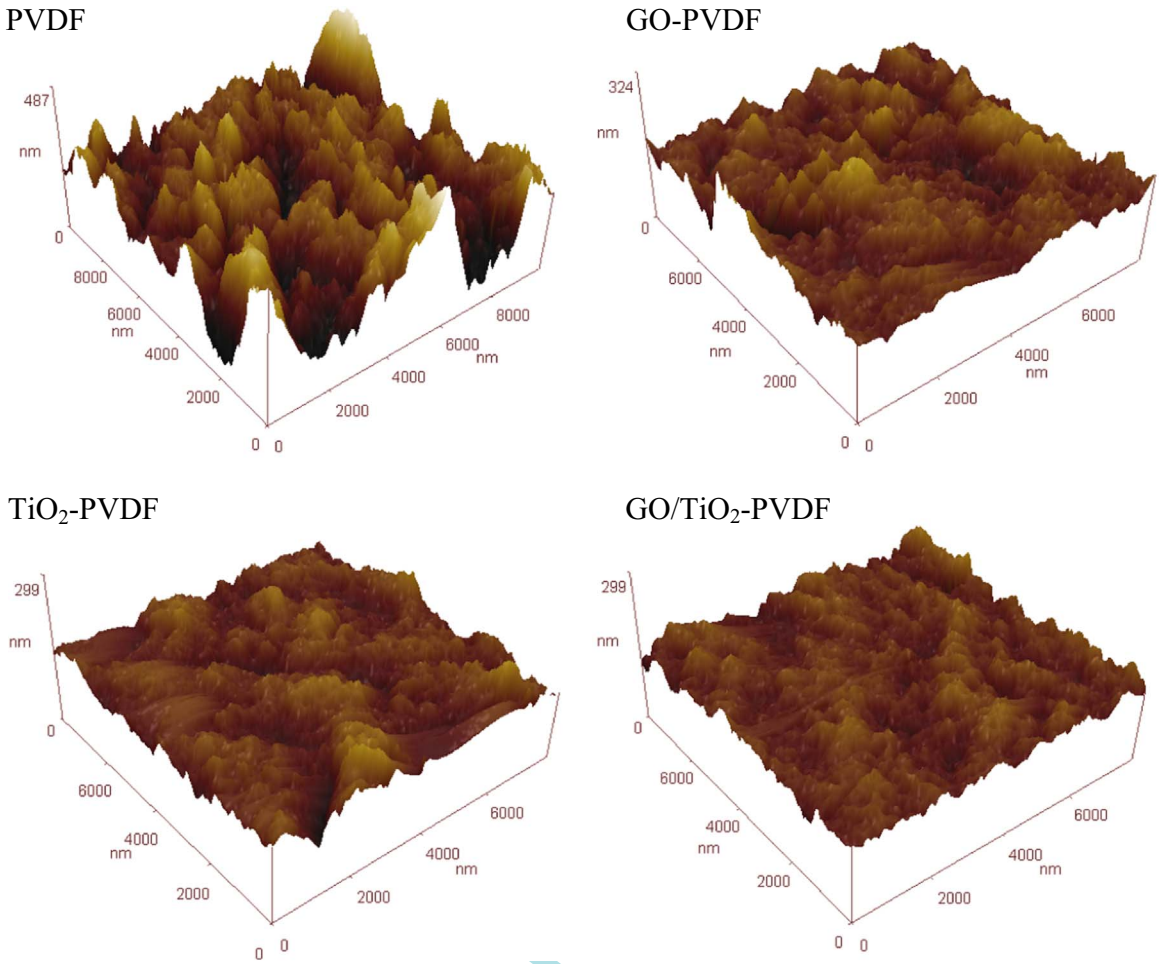

Fig. 5. Three-dimensional AFM images of various membranes.

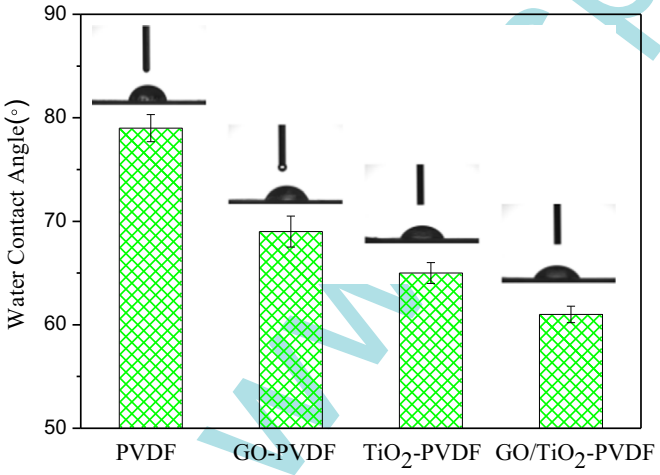

Fig. 6. Water contact angle of various membranes.

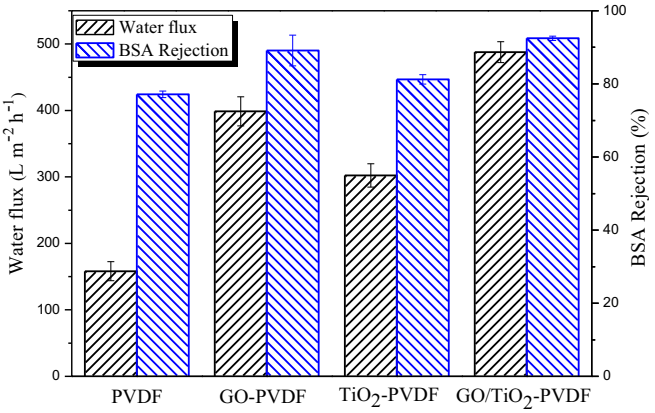

Fig. 7. Pure water flux and BSA rejection of vaious membranes.

3.4. *Permeation and separation properties of membranes*

The results of membrane performance concerning the pure water permeation flux and BSA rejection were illustrated in Fig. 7, which suggested an obvious trend that all the hybrid membranes supplemented with inorganic nanomaterials revealed higher water permeation fluxes and higher separation efficiencies compared with pristine PVDF membranes. According to Fig. 7, the pure water flux of GO/TiO_2-PVDF membranes was 487.8 L m^{-2} h^{-1}, being 208% higher than that of PVDF membranes (158.1 L m^{-2} h^{-1}), 22% higher than that of GO-PVDF membranes (398.7 L m^{-2} h^{-1}) and 61% higher than that of TiO_2-PVDF membranes (302.4 L m^{-2} h^{-1}). This improvement in water flux may be due to the coupling effects of the following two main parameters: 1) Supplementation of the membrane matrix with GO, TiO_2 and GO/TiO_2 nanomaterials would make the membrane more hydrophilic, which facilitates the water molecules to pass through the membrane [49]. As the contact angle shown in Fig. 6, the increasing trend of contact angle was almost in accord with the water permeability promotion. 2)

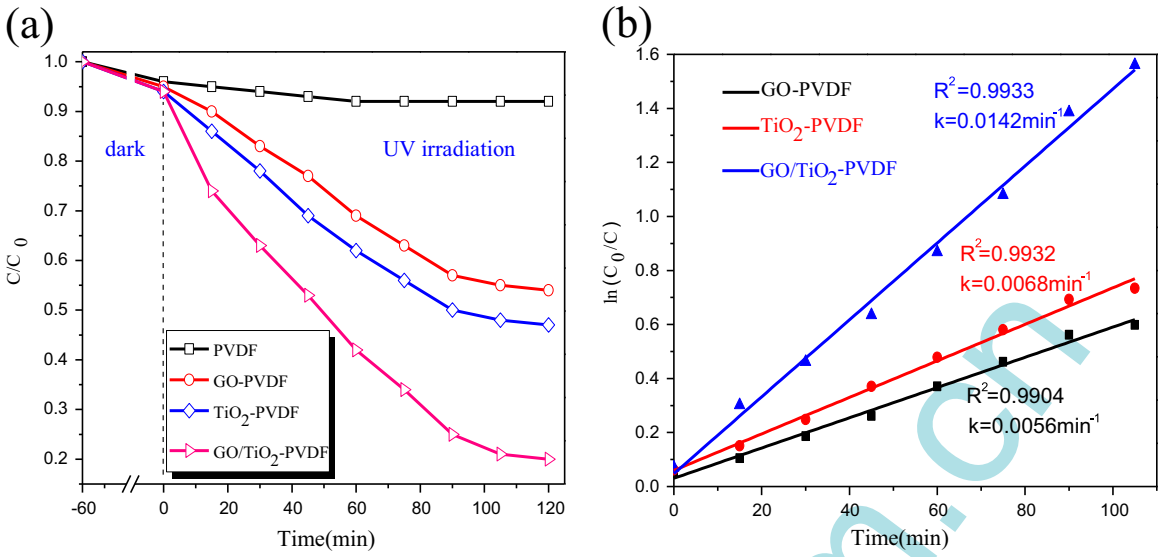

Fig. 8. Photodegradation of BSA under UV light irradiation (a) and the corresponding kinetic linear simulation curves (b) for vaious membranes.

The formation of advantageous porous surfaces of all the hybrid membranes due to the quick exchange between non-solvent and solvent during the phase inversion process was also responsible for the water permeability promotion. Based on the results of porosity and mean pore size of membranes presented in Table 2, all of the hybrid membranes displayed an increase in porosity and mean pore size compared with that of pristine PVDF membranes, which undoubtedly benefited the water permeability [70]. Hence, the increased hydrophilicity and enhanced structure (pore size and porosity) of membranes accounted for promoting the pure water flux of membranes [75]. The increased hydrophilicity, together with the bigger pore and higher porosity enabled that the GO/TiO_2-PVDF membrane presented superior pure water flux over the other three control membranes.

The BSA rejection properties, of the pristine and hybrid membranes, were also presented in Fig. 7. As can be seen, the rejection parameter of the hybrid membranes was increased with supplementation of inorganic nanomaterials into membrane matrix. A minimum value of 77.1% of BSA rejection presented for pristine PVDF membranes and a maximum value of 92.5% presented for GO/TiO_2-PVDF membranes, implying that the tradeoff of membranes could be broken through incorporating specific inorganic nanomaterials such as GO, TiO_2 and GO/TiO_2, which was in good agreement with literature [56,71]. This behavior may be explained by a combination of the small pore size of the skin layer of membranes (which was less than the size of BSA [76]) and the enhanced hydrophilicity based on the principle of the interfacial hydration layer as protective barrier which could decrease the interaction between BSA and membrane surface so as to hinder the protein molecules to penetrate through the hybrid membrane during the fouling or BSA filtration operating [61,63].

3.5. Photocatalytic property of membranes

The photocatalytic property of GO/TiO_2-PVDF membranes was assessed by monitoring the degradation of BSA solution first in darkness and then under UV irradiation. As references, photodegradation of PVDF membranes, GO-PVDF membranes and TiO_2-PVDF membranes was also investigated under identical conditions. Before commencing the UV lamp, the solution was in darkness for 60 min to establish adsorption equilibrium and thus served as a control to study the photocatalytic effect. As shown in Fig. 8a, almost no photodegradation activity of BSA under UV was observed for pristine PVDF membranes. This suggested that PVDF itself did not have any photocatalytic capability. In contrast, supplementation of the membrane matrix with GO, TiO_2 and GO/TiO_2 resulted in enhanced photoactivity activity under UV light. GO/TiO_2-PVDF membranes owned 80% of photodegradation efficiency toward BSA, 53% for TiO_2-PVDF membranes, and 46% for GO-PVDF membranes within the same period. Note that GO-PVDF membranes showed a very similar photocatalytic property to TiO_2-PVDF membranes. This suggested that GO, as a semiconductor and

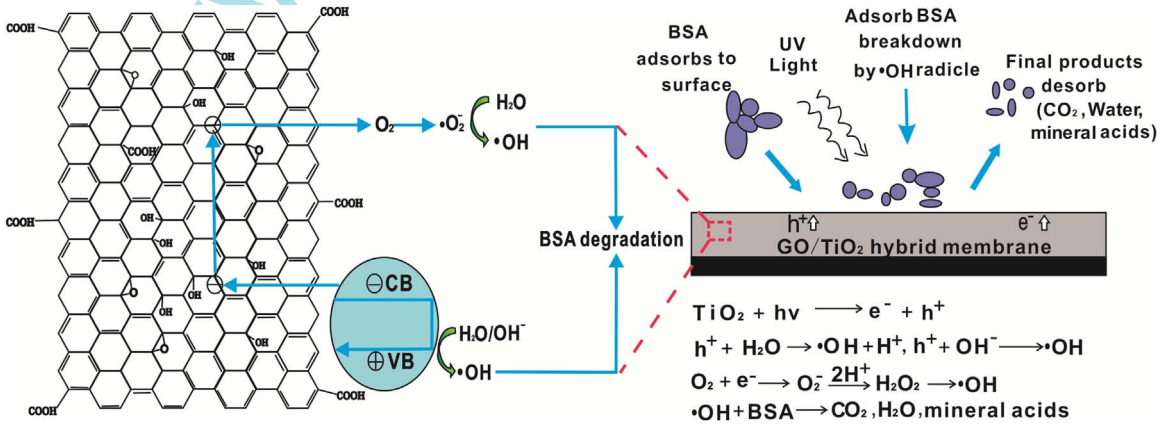

Fig. 9. Possible photocatalysis mechanism and process of GO/TiO_2-PVDF membranes [29,77].

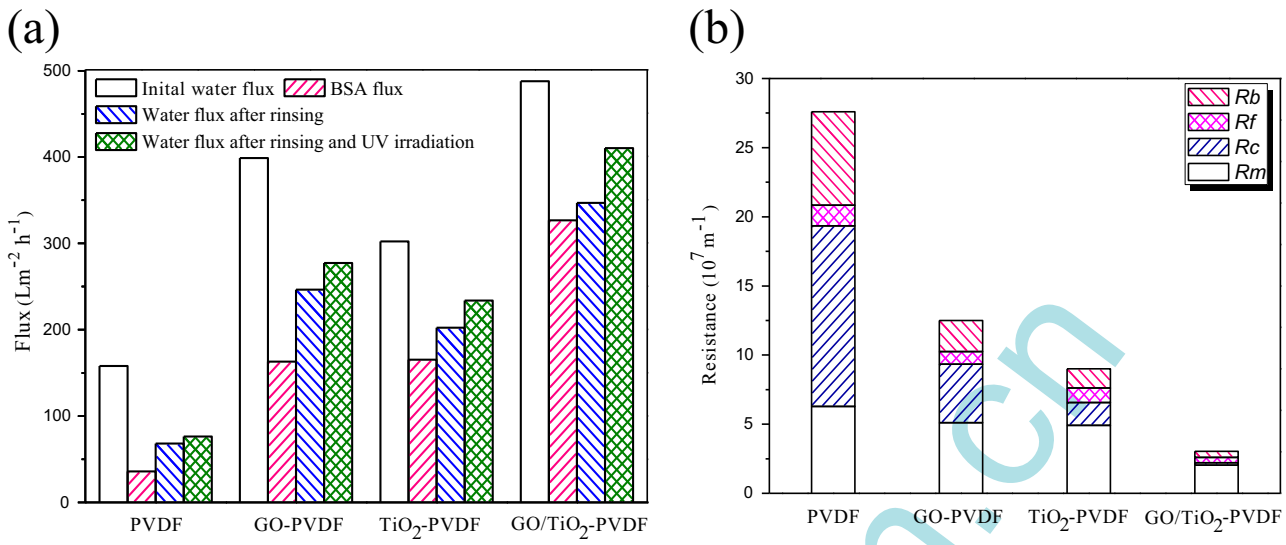

Fig. 10. (a) Equilibrium flux values at different process (fresh, after fouling, rinsing, and UV irradiation) and (b) analysis of the filtration resistances for vaious membranes.

photocatalyst itself, has a band-gap energy similar to TiO_2, which has also been verified by Mi et al. [55]. Superior photocatalytic performance was obtained for GO/TiO_2-PVDF membranes, which could be attributed to the integration of TiO_2 and GO. As reported by previous investigations [55,62], the integration of TiO_2 and GO could be beneficial for the decrease in the charge recombination effect and eventually enhance the photocatalytic efficiency.

To further quantify photocatalytic performance of membranes, the kinetics of BSA photodegradation was fitted according to pseudo-first-order reaction kinetics equation of $\ln(C_0/C)=kt$, where k is the apparent rate constant, and C_0 and C are the initial and reaction concentration of BSA solution, respectively. Fig. 8b traced the apparent rate constants of membranes calculated from Fig. 8a and the high coefficient of determination ($R^2 > 0.99$) signified good fit to pseudo-first-order rate kinetics. It was observed that the kinetics for GO/TiO_2-PVDF membranes was about 108% and 153% faster than those for the TiO_2-PVDF membranes and GO-PVDF membranes, respectively. The higher rate constant associated with GO/TiO_2-PVDF membranes could be related to the role of GO as an acceptor of the activated electrons from TiO_2, thereby reducing carrier recombination and eventually achieving an enhanced photocatalytic efficiency [62].

The possible photodegradation mechanism of BSA was detailed elsewhere [29,77], as described in Fig. 9. Basically, under UV irradiation, TiO_2 can be excited to generate photo-electrons (e^-) and holes (h^+). The electrons can be captured by the oxygen molecule (O_2) on the TiO_2 surface to produce O_2^-, HO_2^-, H_2O_2 and hydroxyl radical (•OH). And, the holes can interact with water molecule and hydroxyl group (OH^-) to produce hydroxyl radical •OH. The •OH can degrade most of the complex organic compounds [29]. Damodar et al. [29] studied the UV photodegradation of BSA and reported a FRR of 98% for BSA filtration by 30 min UV irradiation using a PVDF/TiO_2 membrane. Yang et al. [77] have also observed photodegradation of BSA under near UV (365 nm) irradiation and suggested that the degradation of BSA happened in two steps: first to small fragments, then further mineralized to small inorganic molecule. The efficient photocatalytic property has a beneficial effect in mitigating membrane fouling due to the photocatalytic oxidation of foulants, which guaranteed that GO/TiO_2-PVDF membranes can maintain high permeate flux for longer time than traditional membranes.

3.6. Fouling analysis and self-cleaning evaluation of membranes

The fouling behavior towards GO/TiO_2-PVDF membranes was investigated using filtration of 1.0 g L^{-1} BSA solution and its performance on flux decline values was monitored during fouling. Fig. 10a traced the equilibrium flux values of membranes before and after fouling and after the cleaning by rinsing and UV exposure. It can be observed that flux declined sharply in BSA due to fouling. Nevertheless, the hybrid membranes showed higher fluxes and lower flux reduction coefficients as compared to pristine PVDF membranes, suggesting the enhancement of antifouling performance. With simple water rinsing, the permeate flux of membranes increased due to the removal of loosely bound BSA by mere shear force. However, it was not enough to regain the original attributes of membranes. After a supplementary UV irradiation following water cleaning, further flux increment was observed for hybrid membranes but not for pristine PVDF membranes. A maximum increment in flux recovery was presented for GO/TiO_2-PVDF membranes, indicating that the activation of photocatalytic property and the photo-induced hydrophilicity of GO/TiO_2-PVDF membranes under UV could benefit for removing strongly bound BSA and endow the membrane with self-cleaning property. Note that the fluxes did not recover completely for all the membranes. This may be ascribed to the BSA blocking for membrane pores, agreeing with the experience of Damodar et al. [29] and Moghadam et al. [78]. However, the effect of UV continuous irradiation on membrane flux performance has not been investigated yet in this paper, and further research is necessary to have a more detailed insight. Nonetheless, it is evident that GO/TiO_2-PVDF membranes showed better antifouling performance over the other membranes under UV static irradiation.

The different filtration resistances of membranes were calculated according to the above mentioned equilibrium flux values, as depicted in Fig. 10b. It was observed that the total resistance (R_{tot}) of GO/TiO_2-PVDF membranes was lowest as compared to other membranes. Detailed analysis showed that the intrinsic membrane resistance (R_m) was consistent with the results of the pore sizes of membranes listed in Table 2. This outcome may be due to the fact that the R_m was highly dependent upon the pore sizes of membranes [13]. The cake resistance (R_c) was related to the hydrophilicity and roughness of membranes and the R_c decreased with the improvement in hydrophilicity and the change in the roughness of hybrid membranes. The fouling resistance (R_f), which

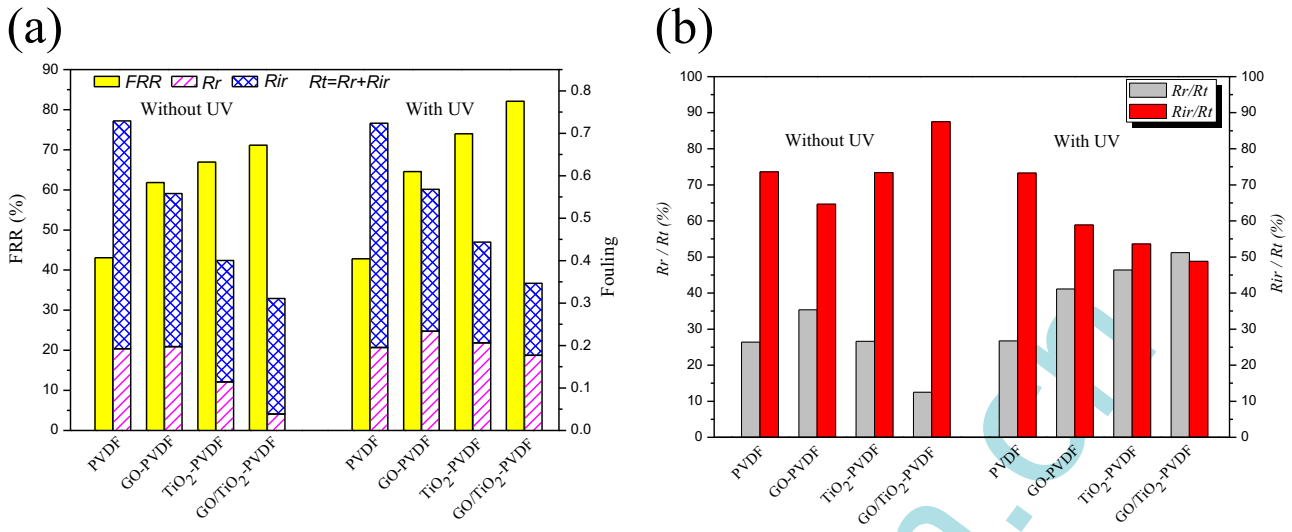

Fig. 11. (a) Water flux recovery (*FRR*) and fouling resistance of membranes; (b) the ratio of reversible fouling (*Rr*) and irreversible fouling (*Rir*) to the total fouling (*Rt*=*Rr*+*Rir*), respectively.

was caused by the strongly bound protein and strongly depended on the membrane self-cleaning capability, was remarkably alleviated by the supplement of GO/TiO_2. The reduction in R_f under UV may be ascribed to the self-cleaning mechanism and the improved hydrophilicity of GO/TiO_2-PVDF membranes. The GO/TiO_2-PVDF membrane had the least block resistance (R_b) because of the photodegradation of BSA at the surface or periphery of pores and the improvement in membrane hydrophilicity. Concurring with permeability and hydrophilicity trends, the GO/TiO_2-PVDF membrane showed the least total and fractional resistances, suggesting the best self-cleaning (antifouling) property.

To comprehensively monitor membrane fouling, two important parameters of water flux recovery ratio (*FRR*) and fouling ratio (*Rt*) were introduced and evaluated by employing Eqs. (8)–(11). Fig. 11 illustrated values of *FRR* and *Rt* for all of membranes with and without UV irradiation following BSA fouling. Generally, a higher *FRR* value refers to a superior antifouling character of membranes. As can be clearly seen from Fig. 11, *FRR* of all hybrid membranes was clearly higher than that of pristine PVDF membranes. This indicated the improved antifouling characteristic of the hybrid membranes. *FRR* of pristine PVDF membranes without UV irradiation was as low as 43.1%, implying a poor antifouling property. Supplementation of the membrane with GO, TiO_2 and GO/TiO_2 tended to considerably increase *FRR* of the hybrid membranes and the maximum *FRR* value (71.1%) was observed for GO/TiO_2-PVDF membranes without UV irradiation. The amelioration of

Table 3
Comparison of the comprehensive performance for inorganic nanomaterial-PVDF hybrid membranes reported in the literatures and the GO/TiO_2-PVDF membrane in this work (concentration of foulants may be different).

Membrane	Optimum dosage (wt%)	Contact age (deg.)	Water flux ($L\,m^{-2}\,h^{-1}$)	Rejection (%)	Foulant	Photocatalytic property (%)	Water flux recovery (%) UV	Without UV	Ref.
PVDF-ZnO[a]	1.5	63.2	147.2	~93	RW[b]	~85	~88.3	–	13
PVDF-Al_2O_3	2	81.1	134.4	93.4	BSA	–	–	~40	16
PVDF-Fe_3O_4	25	–	65.6	93	BSA	–	–	55.2	23
PVDF-SiO_2	3	56.7	198	94.5	BSA	–	–	–	14
PVDF-TiO_2[c]	0.5	74	~240	~85	NOM[d]	–	1 h 2 h 4 h 69 71 90	54	20
PVDF-TiO_2[a]	2	86.1	84	–	BSA	~75	98.7	97.5	29
PVDF-TiO_2[a]	1.5	–	392.8	–	MB[e]	–	0.5 h 1 h 95 100	91.3	21
PVDF-TiO_2[c]	4	60.7	103.5	85.6	BSA	–	96.9	60.2	78
PVDF-TiO_2[c]	25	~64	150	–	BSA	–	~100	~93	19
PVDF-OMWCNTs	1	66.8	119	86.9	BSA	–	–	72.8	63
PVDF-GO	1	66.4	163	83.7	BSA	–	–	85.1	63
PVDF-GO/ OMWCNTs	1	48.6	203	81.6	BSA	–	–	80.4	63
PVDF-GO	2	60.5	26.5	–	BSA	–	–	88.6	43
PVDF-GO	0.5	~68	104.3	85	BSA	–	–	–	75
PVDF-GO	16	60.7	457.9	91.1	BSA	–	–	96.4	44
PVDF-GO	1	51	401.4	55	BSA	–	–	–	61
PVDF-rGO/TiO_2	1.05	69	221	99	BSA	–	–	95	49
PVDF-GO/TiO_2[a]	1	61	487.8	92.5	BSA	80	82.1	71.1	This work

[a] The type of UV irradiation experiments was UV static irradiation.
[b] Reclaimed water.
[c] The type of UV irradiation experiments was UV continuous irradiation.
[d] Natural organic matter.
[e] Methylene blue.

antifouling behavior of the hybrid membranes can be attributed to the increased membrane hydrophilicity and the smoother membrane surface (see Table 2) compared with pristine PVDF membranes. Compared with the hybrid membranes without UV irradiation, *FRR* for the hybrid membranes with UV irradiation further increased due to the possible photocatalytic degradation of BSA [29]. In the best case, related to GO/TiO_2-PVDF membranes, *FRR* increased from 71.1% to 82.1%. This phenomenon indicated the improvement in antifouling property of membranes by the GO/TiO_2 and UV irradiation which benefited for membrane self-cleaning, agreeing with the experience of Mendret et al. [19] and Moghadam et al. [78]. Furthermore, *Rt* ($Rt=Rr+Rir$) of all the hybrid membranes was obviously lower than that of pristine PVDF membranes and followed the sequence of PVDF membranes > GO-PVDF membranes > TiO_2-PVDF membranes > GO/TiO_2-PVDF membranes. This observation was consistent with the results of membrane hydrophilicity and suggested that the enhanced membrane hydrophilicity as a result of inorganic nanomaterials supplementation and UV irradiation was beneficial for endowing membrane with antifouling tendency.

In more detail, membrane fouling was mainly related to the loose protein adsorption on membrane surface (reversible resistance) and protein deposition on the surface or entrapment within the pores (irreversible resistance) [61]. As shown in Fig. 11b, the percentages of reversible fouling in total fouling (*Rr*/*Rt*) were 26.4%, 35.4%, 26.6% and 12.5% for PVDF, GO-PVDF, TiO_2-PVDF and GO/TiO_2-PVDF membranes without UV irradiation, while these values were increased to 26.7%, 41.1%, 46.4% and 51.2% for PVDF, GO-PVDF, TiO_2-PVDF and GO/TiO_2-PVDF membranes with UV irradiation, respectively. On the contrary, the percentages of irreversible fouling in total fouling (*Rir*/*Rt*) of the hybrid membranes further decreased with UV irradiation as compared to the hybrid membranes without UV irradiation. The phenomena indicated that *Rir* dominates the total fouling and membrane fouling could be effectively mitigated under UV irradiation for the hybrid membranes due to the photocatalytic oxidation of BSA [77]. In summary, all of the obtained results indicated that GO/TiO_2-PVDF membranes had better photocatalytic antifouling behavior over the other membranes and could be a well candidate for application in antifouling fields.

In addition, comparison of the comprehensive performance for inorganic nanomaterial-PVDF hybrid membranes reported in the literatures and GO/TiO_2-PVDF membranes in this work (Table 3) indicated that the GO/TiO_2-PVDF membrane presented a promising performance compared with the other inorganic nanomaterial-PVDF hybrid membranes, which illustrates that such high-performance multifunctional membranes may broaden the horizon of membrane-based water and wastewater treatment technology.

4. Conclusions

In summary, a novel multifunctional GO/TiO_2-PVDF hybrid membrane was successfully fabricated via the phase inversion technique by supplementing GO/TiO_2 nanocomposites into the PVDF matrix. The following can be highlighted from the experimental study:

(1) The GO/TiO_2-PVDF membrane exhibited an ideal morphology, *i.e.* lower surface roughness, higher surface pore size and porosity and more porous structure compared with pristine PVDF, GO-PVDF and TiO_2-PVDF membranes resulting in enhanced antifouling properties and separation performance.
(2) The GO/TiO_2-PVDF membrane exhibited significant improvement in hydrophilicity and water permeability, where the pure water flux of GO/TiO_2-PVDF membranes with a water contact angle of $61 \pm 0.8^\circ$ reached 487.8 L m^{-2} h^{-1} in comparison to 158.1 L m^{-2} h^{-1} for pristine PVDF membranes with a water contact angle of $79 \pm 1.3^\circ$, implying the improved hydrophilicity and ameliorative membrane structure due to the implantation of GO/TiO_2 in PVDF matrix.
(3) For the GO/TiO_2-PVDF membrane, there was a 51% and 74% increase in photodegradation efficiency and a 108% and 153% increase in photodegradation kinetics toward BSA, compared with PVDF membranes supplemented with TiO_2 and GO, respectively, suggesting that the integration of TiO_2 and GO had a synergistic effect and improved the induced effect of photocatalytic property.
(4) After a supplementary UV static irradiation following water cleaning, the GO/TiO_2-PVDF membrane enabled to reach a high recovery of membrane performance after fouling, confirming their self-cleaning ability.

Hence, it can be concluded that the GO/TiO_2-PVDF membrane may present a next generation of high-performance multifunctional membrane for fouling mitigation in practical water treatment.

Acknowledgments

The work was funded by the Petrochemical Joint Funds of National Natural Science Fund Committee – China National Petroleum Corporation (U1362108), the Natural Science Foundation of Tianjin (16JCZDJC36400, 15JCZDJC38500) and the Science and Technology Plans of Tianjin (15PTSYJC00230).

Nomenclature

A	effective area of membranes (m^2)
Q	volume of the permeate pure water (L)
T	permeation time (h)
J	permeation flux of membrane for pure water (L m^{-2} h^{-1})
C_P	concentration of BSA in permeate stream (g L^{-1})
C_F	concentration of BSA in feed stream (g L^{-1})
R	BSA rejection (%)
Jw_1	pure water flux through a clean membrane (L m^{-2} h^{-1})
Jp	permeate flux (L m^{-2} h^{-1})
Jrw	pure water flux after removing loose bound protein (L m^{-2} h^{-1})
Jw_2	pure water flux after cleaning membranes (L m^{-2} h^{-1})
TMP	transmembrane pressure (MPa)
Ra	mean roughness (nm)
Rq	root mean square roughness (nm)
μ	water viscosity (Pa s)
R_{tot}	the total filtration resistance (m^{-1})
R_m	intrinsic membrane resistance (m^{-1})
R_c	cake resistance (m^{-1})
R_f	fouling resistance (m^{-1})
R_b	block resistance (m^{-1})
k	the apparent rate constant (%)
C_0	the initial concentration of BSA solution during photodegradation (g L^{-1})
C	the reaction concentration of BSA solution during photodegradation (g L^{-1})

FRR	flux recovery ratio (%)
Rt	total fouling ratio (%)
Rr	reversible fouling ratio (%)
Rir	irreversible fouling ratio (%)
Rr*/*Rt	the percentage of reversible fouling in total fouling (%)
Rir*/*Rt	the percentage of irreversible fouling in total fouling (%)
GO	graphene oxide
rGO	reduced graphene oxide
PVDF	polyvinylidene fluoride
PVP	polyvinyl pyrrolidone
DMAc	N,N-dimethylacetamide
BSA	bovine serum albumin
SEM	field emission scanning electron microscopy
TEM	transmission electron microscopy
HRTEM	high-resolution transmission electron microscopy
XRD	X-ray Diffraction
XPS	X-Ray photoelectron spectroscopy
EDX	energy dispersive X-ray
AFM	atomic force microscope

References

[1] L. Yang, B. Tang, P. Wu, UF membrane with highly improved flux by hydrophilic network between graphene oxide and brominated poly (2,6-dimethyl-1,4-phenylene oxide), J. Mater. Chem. A 2 (2014) 18562–18573.

[2] F. Qu, H. Liang, J. Zhou, J. Nan, S. Shao, J. Zhang, G. Li, Ultrafiltration membrane fouling caused by extracellular organic matter (EOM) from *Microcystis aeruginosa*: effects of membrane pore size and surface hydrophobicity, J. Membr. Sci. 449 (2014) 58–66.

[3] S. Balta, A. Sotto, P. Luis, L. Benea, B. Van der Bruggen, J. Kim, A new outlook on membrane enhancement with nanoparticles: the alternative of ZnO, J. Membr. Sci. 389 (2012) 155–161.

[4] X. Li, X. Fang, R. Pang, J. Li, X. Sun, J. Shen, W. Han, L. Wang, Self-Assembly of TiO_2 nanoparticles around the pores of PES ultrafiltration membrane for mitigating organic fouling, J. Membr. Sci. 467 (2014) 226–235.

[5] F. Liu, N.A. Hashim, Y. Liu, M. Abed, K. Li, Progress in the production and modification of PVDF membranes, J. Membr. Sci. 375 (2011) 1–27.

[6] B.S. Lalia, V. Kochkodan, R. Hashaikeh, N. Hilal, A review on membrane fabrication: structure, properties and performance relationship, Desalination 326 (2013) 77–95.

[7] G.-D. Kang, Y.-M. Cao, Application and modification of poly (vinylidene fluoride)(PVDF) membranes-a review, J. Membr. Sci. 463 (2014) 145–165.

[8] T. Noeiaghaei, J.-O. Kim, S.-R. Chae, Recent advances in nano-hybrid membranes for advanced water treatment, Curr. Org. Chem. 18 (2014) 2381–2404.

[9] L.Y. Ng, A.W. Mohammad, C.P. Leo, N. Hilal, Polymeric membranes incorporated with metal/metal oxide nanoparticles: a comprehensive review, Desalination 308 (2013) 15–33.

[10] M. Hadidi, A.L. Zydney, Fouling behavior of zwitterionic membranes: impact of electrostatic and hydrophobic interactions, J. Membr. Sci. 452 (2014) 97–103.

[11] D. Rana, T. Matsuura, Surface modifications for antifouling membranes, Chem. Rev. 110 (2010) 2448–2471.

[12] P. Goh, B. Ng, W. Lau, A. Ismail, Inorganic nanomaterials in polymeric ultrafiltration membranes for water treatment, Sep. Purif. Rev. 44 (2015) 216–249.

[13] J. Hong, Y. He, Polyvinylidene fluoride ultrafiltration membrane blended with nano-ZnO particle for photo-catalysis self-cleaning, Desalination 332 (2014) 67–75.

[14] S. Zhang, R. Wang, S. Zhang, G. Li, Y. Zhang, Treatment of wastewater containing oil using phosphorylated silica nanotubes (PSNTs)/polyvinylidene fluoride (PVDF) composite membrane, Desalination 332 (2014) 109–116.

[15] J. Garcia-Ivars, M.-I. Alcaina-Miranda, M.-I. Iborra-Clar, J.-A. Mendoza-Roca, L. Pastor-Alcañiz, Enhancement in hydrophilicity of different polymer phase-inversion ultrafiltration membranes by introducing PEG/Al_2O_3 nanoparticles, Sep. Purif. Technol. 128 (2014) 45–57.

[16] F. Liu, M.M. Abed, K. Li, Preparation and characterization of poly (vinylidene fluoride)(PVDF) based ultrafiltration membranes using nano γ-Al_2O_3, J. Membr. Sci. 366 (2011) 97–103.

[17] K. De Sitter, C. Dotremont, I. Genné, L. Stoops, The use of nanoparticles as alternative pore former for the production of more sustainable polyethersulfone ultrafiltration membranes, J. Membr. Sci. 471 (2014) 168–178.

[18] R. Pang, X. Li, J. Li, Z. Lu, X. Sun, L. Wang, Preparation and characterization of ZrO_2/PES hybrid ultrafiltration membrane with uniform ZrO_2 nanoparticles, Desalination 332 (2014) 60–66.

[19] J.P. Méricq, J. Mendret, S. Brosillon, C. Faur, High performance PVDF-TiO_2 membranes for water treatment, Chem. Eng. Sci. 123 (2015) 283–291.

[20] H. Song, J. Shao, Y. He, B. Liu, X. Zhong, Natural organic matter removal and flux decline with PEG-TiO_2-doped PVDF membranes by integration of ultrafiltration with photocatalysis, J. Membr. Sci. 405 (2012) 48–56.

[21] H. Ngang, B. Ooi, A. Ahmad, S. Lai, Preparation of PVDF-TiO_2 mixed-matrix membrane and its evaluation on dye adsorption and UV-cleaning properties, Chem. Eng. J. 197 (2012) 359–367.

[22] J. Dasgupta, S. Chakraborty, J. Sikder, R. Kumar, D. Pal, S. Curcio, E. Drioli, The effects of thermally stable titanium silicon oxide nanoparticles on structure and performance of cellulose acetate ultrafiltration membranes, Sep. Purif. Technol. 133 (2014) 55–68.

[23] Z.-Q. Huang, F. Zheng, Z. Zhang, H.-T. Xu, K.-M. Zhou, The performance of the PVDF-Fe_3O_4 ultrafiltration membrane and the effect of a parallel magnetic field used during the membrane formation, Desalination 292 (2012) 64–72.

[24] J.-H. Li, X.-S. Shao, Q. Zhou, M.-Z. Li, Q.-Q. Zhang, The double effects of silver nanoparticles on the PVDF membrane: Surface hydrophilicity and antifouling performance, Appl. Surf. Sci. 265 (2013) 663–670.

[25] F. Liu, B.-R. Ma, D. Zhou, Y.-H. Xiang, L.-X. Xue, Breaking through tradeoff of Polysulfone ultrafiltration membranes by zeolite 4A, Microporous Mesoporous Mater. 186 (2014) 113–120.

[26] Y. Zhang, J. Zhao, H. Chu, X. Zhou, Y. Wei, Effect of modified attapulgite addition on the performance of a PVDF ultrafiltration membrane, Desalination 344 (2014) 71–78.

[27] X. Wang, Z. Li, J. Shi, Y. Yu, One-dimensional titanium dioxide nanomaterials: nanowires, nanorods, and nanobelts, Chem. Rev. 114 (2014) 9346–9384.

[28] X. Zhang, T. Zhang, J. Ng, D.D. Sun, High-performance multifunctional TiO_2 nanowire ultrafiltration membrane with a hierarchical layer structure for water treatment, Adv. Funct. Mater. 19 (2009) 3731–3736.

[29] R.A. Damodar, S.-J. You, H.-H. Chou, Study the self cleaning, antibacterial and photocatalytic properties of TiO_2 entrapped PVDF membranes, J. Hazard. Mater. 172 (2009) 1321–1328.

[30] S. Leong, A. Razmjou, K. Wang, K. Hapgood, X. Zhang, H. Wang, TiO_2 based photocatalytic membranes: a review, J. Membr. Sci. 472 (2014) 167–184.

[31] Y. Teow, A. Ahmad, J. Lim, B. Ooi, Preparation and characterization of PVDF/TiO_2 mixed matrix membrane via in situ colloidal precipitation method, Desalination 295 (2012) 61–69.

[32] S. Anandan, T. Narasinga Rao, M. Sathish, D. Rangappa, I. Honma, M. Miyauchi, Superhydrophilic graphene-loaded TiO_2 thin film for self-cleaning applications, ACS Appl. Mater. Interfaces 5 (2012) 207–212.

[33] Y. Chen, W. Huang, D. He, Y. Situ, H. Huang, Construction of heterostructured g-C_3N_4/Ag/TiO_2 microspheres with enhanced photocatalysis performance under visible-light irradiation, ACS Appl. Mater. Interfaces 6 (2014) 14405–14414.

[34] G. Wu, M.A. Nelson, N.H. Mack, S. Ma, P. Sekhar, F.H. Garzon, P. Zelenay, Titanium dioxide-supported non-precious metal oxygen reduction electrocatalyst, Chem. Commun. 46 (2010) 7489–7491.

[35] Y. Li, L. Zhu, Y. Guo, H. Song, Z. Lou, Z. Ye, A new type of hybrid nanostructure: complete photo-generated carrier separation and ultrahigh photocatalytic activity, J. Mater. Chem. A 2 (2014) 14245–14250.

[36] S. Linley, Y. Liu, C.J. Ptacek, D.W. Blowes, F.X. Gu, Recyclable graphene oxide-supported titanium dioxide photocatalysts with tunable properties, ACS Appl. Mater. Interfaces 6 (2014) 4658–4668.

[37] Y. Jiang, W.-N. Wang, P. Biswas, J.D. Fortner, Facile aerosol synthesis and characterization of ternary crumpled graphene-TiO_2-magnetite nanocomposites for advanced water treatment, ACS Appl. Mater. Interfaces 6 (2014) 11766–11774.

[38] G. Wu, K.L. More, P. Xu, H.-L. Wang, M. Ferrandon, A.J. Kropf, D.J. Myers, S. Ma, C.M. Johnston, P. Zelenay, A carbon-nanotube-supported graphene-rich non-precious metal oxygen reduction catalyst with enhanced performance durability, Chem. Commun. 49 (2013) 3291–3293.

[39] M. Ioanálonescu, 3D boron doped carbon nanorods/carbon-microfiber hybrid composites: synthesis and applications in a highly stable proton exchange membrane fuel cell, J. Mater. Chem. 21 (2011) 18195–18198.

[40] J. Wang, G. Yin, Y. Shao, Z. Wang, Y. Gao, Investigation of further improvement of platinum catalyst durability with highly graphitized carbon nanotubes support, J. Phys. Chem. C 112 (2008) 5784–5789.

[41] X. Huang, X. Qi, F. Boey, H. Zhang, Graphene-based composites, Chem. Soc. Rev. 41 (2012) 666–686.

[42] Q. Xiang, J. Yu, M. Jaroniec, Graphene-based semiconductor photocatalysts, Chem. Soc. Rev. 41 (2012) 782–796.

[43] C. Zhao, X. Xu, J. Chen, F. Yang, Effect of graphene oxide concentration on the morphologies and antifouling properties of PVDF ultrafiltration membranes, J. Environ. Chem. Eng. 1 (2013) 349–354.

[44] Z. Wang, H. Yu, J. Xia, F. Zhang, F. Li, Y. Xia, Y. Li, Novel GO-blended PVDF ultrafiltration membranes, Desalination 299 (2012) 50–54.

[45] J. Wang, Y. Li, X. Sun, Challenges and opportunities of nanostructured materials for aprotic rechargeable lithium-air batteries, Nano Energy 2 (2013) 443–467.

[46] Z. Jiang, J. Wang, L. Meng, Y. Huang, L. Liu, A highly efficient chemical sensor material for ethanol: Al_2O_3/graphene nanocomposites fabricated from graphene oxide, Chem. Commun. 47 (2011) 6350–6352.

[47] T.N. Lambert, C.A. Chavez, B. Hernandez-Sanchez, P. Lu, N.S. Bell, A. Ambrosini, T. Friedman, T.J. Boyle, D.R. Wheeler, D.L. Huber, Synthesis and characterization of titania-graphene nanocomposites, J. Phys. Chem. C 113 (2009) 19812–19823.

[48] S. Morales-Torres, L.M. Pastrana-Martínez, J.L. Figueiredo, J.L. Faria, A.M. Silva, Design of graphene-based TiO_2 photocatalysts -a review, Environ. Sci. Pollut. Res. 19 (2012) 3676–3687.
[49] M. Safarpour, A. Khataee, V. Vatanpour, Effect of reduced graphene oxide/TiO_2 nanocomposite with different molar ratios on the performance of PVDF ultrafiltration membranes, Sep. Purif. Technol. 140 (2015) 32–42.
[50] J. Liu, H. Bai, Y. Wang, Z. Liu, X. Zhang, D.D. Sun, Self-assembling TiO_2 nanorods on large graphene oxide sheets at a two-phase interface and their anti-recombination in photocatalytic applications, Adv. Funct. Mater. 20 (2010) 4175–4181.
[51] P. Gao, D.D. Sun, Ultrasonic preparation of hierarchical graphene-oxide/TiO_2 composite microspheres for efficient photocatalytic hydrogen production, Chem.-Asian J. 8 (2013) 2779–2786.
[52] P. Gao, Z. Liu, M. Tai, D.D. Sun, W. Ng, Multifunctional graphene oxide-TiO_2 microsphere hierarchical membrane for clean water production, Appl. Catal. B 138 (2013) 17–25.
[53] C.P. Athanasekou, S. Morales-Torres, V. Likodimos, G.E. Romanos, L. M. Pastrana-Martinez, P. Falaras, J.L. Faria, J.L. Figueiredo, A.M. Silva, Prototype composite membranes of partially reduced graphene oxide/TiO_2 for photocatalytic ultrafiltration water treatment under visible light, Appl. Catal. B 158 (2014) 361–372.
[54] C. Xu, Y. Xu, J. Zhu, Photocatalytic antifouling graphene oxide-mediated hierarchical filtration membranes with potential applications on water purification, ACS Appl. Mater. Interfaces 6 (2014) 16117–16123.
[55] Y. Gao, M. Hu, B. Mi, Membrane surface modification with TiO_2-graphene oxide for enhanced photocatalytic performance, J. Membr. Sci. 455 (2014) 349–356.
[56] M. Safarpour, A. Khataee, V. Vatanpour, Preparation of a novel polyvinylidene fluoride (PVDF) ultrafiltration membrane modified with reduced graphene oxide/titanium dioxide (TiO_2) nanocomposite with enhanced hydrophilicity and antifouling properties, Ind. Eng. Chem. Res. 53 (2014) 13370–13382.
[57] M. Safarpour, V. Vatanpour, A. Khataee, Preparation and characterization of graphene oxide/TiO_2 blended PES nanofiltration membrane with improved antifouling and separation performance, Desalination 393 (2016) 65–78.
[58] M. Kumar, Z. Gholamvand, A. Morrissey, K. Nolan, M. Ulbricht, J. Lawler, Preparation and characterization of low fouling novel hybrid ultrafiltration membranes based on the blends of GO-TiO_2 nanocomposite and polysulfone for humic acid removal, J. Membr. Sci. 506 (2016) 38–49.
[59] C. Shi, L. Chen, Z. Xu, Y. Jiao, Y. Li, C. Wang, M. Shan, Z. Wang, Q. Guo, Monitoring influence of chemical preparation procedure on the structure of graphene nanosheets, Physica E 44 (2012) 1420–1424.
[60] J. Zhang, Z. Xu, M. Shan, B. Zhou, Y. Li, B. Li, J. Niu, X. Qian, Synergetic effects of oxidized carbon nanotubes and graphene oxide on fouling control and antifouling mechanism of polyvinylidene fluoride ultrafiltration membranes, J. Membr. Sci. 448 (2013) 81–92.
[61] Z. Xu, J. Zhang, M. Shan, Y. Li, B. Li, J. Niu, B. Zhou, X. Qian, Organosilane-functionalized graphene oxide for enhanced antifouling and mechanical properties of polyvinylidene fluoride ultrafiltration membranes, J. Membr. Sci. 458 (2014) 1–13.
[62] H. Zhang, X. Lv, Y. Li, Y. Wang, J. Li, P25-graphene composite as a high performance photocatalyst, ACS Nano 4 (2009) 380–386.
[63] J. Zhang, Z. Xu, W. Mai, C. Min, B. Zhou, M. Shan, Y. Li, C. Yang, Z. Wang, X. Qian, Improved hydrophilicity, permeability, antifouling and mechanical performance of PVDF composite ultrafiltration membranes tailored by oxidized low-dimensional carbon nanomaterials, J. Mater. Chem. A 1 (2013) 3101–3111.
[64] Y. Zhao, Z. Xu, M. Shan, C. Min, B. Zhou, Y. Li, B. Li, L. Liu, X. Qian, Effect of graphite oxide and multi-walled carbon nanotubes on the microstructure and performance of PVDF membranes, Sep. Purif. Technol. 103 (2013) 78–83.
[65] J. Ma, Y. Zhao, Z. Xu, C. Min, B. Zhou, Y. Li, B. Li, J. Niu, Role of oxygen-containing groups on MWCNTs in enhanced separation and permeability performance for PVDF hybrid ultrafiltration membranes, Desalination 320 (2013) 1–9.
[66] T. Wu, B. Zhou, T. Zhu, J. Shi, Z. Xu, C. Hu, J. Wang, Facile and low-cost approach towards a PVDF ultrafiltration membrane with enhanced hydrophilicity and antifouling performance via graphene oxide/water-bath coagulation, RSC Adv. 5 (2015) 7880–7889.
[67] L.-J. Zhu, L.-P. Zhu, Y.-F. Zhao, B.-K. Zhu, Y.-Y. Xu, Anti-fouling and anti-bacterial polyethersulfone membranes quaternized from the additive of poly (2-dimethylamino ethyl methacrylate) grafted SiO_2 nanoparticles, J. Mater. Chem. A 2 (2014) 15566–15574.
[68] Y. Xiang, F. Liu, L. Xue, Under seawater superoleophobic PVDF membrane inspired by polydopamine for efficient oil/seawater separation, J. Membr. Sci. 476 (2015) 321–329.
[69] C. Xu, A. Cui, Y. Xu, X. Fu, Graphene oxide-TiO_2 composite filtration membranes and their potential application for water purification, Carbon 62 (2013) 465–471.
[70] S. Xia, M. Ni, Preparation of poly (vinylidene fluoride) membranes with graphene oxide addition for natural organic matter removal, J. Membr. Sci. 473 (2015) 54–62.
[71] H. Rabiee, M.H.D.A. Farahani, V. Vatanpour, Preparation and characterization of emulsion poly (vinyl chloride)(EPVC)/TiO_2 nanocomposite ultrafiltration membrane, J. Membr. Sci. 472 (2014) 185–193.
[72] H. Zhao, L. Wu, Z. Zhou, L. Zhang, H. Chen, Improving the antifouling property of polysulfone ultrafiltration membrane by incorporation of isocyanate-treated graphene oxide. Phys. Chem. Chem. Phys. 15 (2013) 9084–9092.
[73] B. Ganesh, A.M. Isloor, A. Ismail, Enhanced hydrophilicity and salt rejection study of graphene oxide-polysulfone mixed matrix membrane, Desalination 313 (2013) 199–207.
[74] Y. Wei, H.-Q. Chu, B.-Z. Dong, X. Li, S.-J. Xia, Z.-M. Qiang, Effect of TiO_2 nanowire addition on PVDF ultrafiltration membrane performance, Desalination 272 (2011) 90–97.
[75] X. Chang, Z. Wang, S. Quan, Y. Xu, Z. Jiang, L. Shao, Exploring the synergetic effects of graphene oxide (GO) and polyvinylpyrrodione (PVP) on poly (vinylylidenefluoride)(PVDF) ultrafiltration membrane performance, Appl. Surf. Sci. 316 (2014) 537–548.
[76] X. Li, X. Fang, R. Pang, J. Li, X. Sun, J. Shen, W. Han, L. Wang, Self-assembly of TiO_2 nanoparticles around the pores of PES ultrafiltration membrane for mitigating organic fouling, J. Membr. Sci. 467 (2014) 226–235.
[77] G. Yang, Z. Li, Z. Lin, X. Wang, P. Liu, X. Fu, Investigation of TiO_2 photocatalytic degradation of bovine serum albumin, Spectrosc. Spect. Anal. 25 (2005) 1309–1311.
[78] M. Tavakol Moghadam, G. Lesage, T. Mohammadi, J.P. Mericq, J. Mendret, M. Heran, C. Faur, S. Brosillon, M. Hemmati, F. Naeimpoor, Improved antifouling properties of TiO_2/PVDF nanocomposite membranes in UV-coupled ultrafiltration, J. Appl. Polym. Sci. 132 (2014) 41731.